Proceedings of the 21st ICSMGE, Vienna, Austria, 14 – 19 June 2026. Pistrol, Adam & Schweiger (eds.)
Published by: ÖGG, Austrian Society for Geomechanics, Salzburg, Austria, ISBN 978-3-9503898-4-5
https://doi.org/10.53243/ICSMGE2026-428

Thermal volume change of compacted bentonite under high temperatures

Xufei Liu
Department of Structural Engineering; University of California San Diego, lel023@ucsd.edu

Fatemah Behbehani
Department of Civil Engineering College of Engineering and Petroleum Kuwait University Al-Shadadiya, Kuwait, fatemah.behbehani@ku.edu.kw

Yu Lu
College of Civil Engineering, Tongji University, yul204@ucsd.edu

John McCartney
Department of Structural Engineering; University of California San Diego, mccartney@ucsd.edu

ABSTRACT: This study investigates the thermal volumetric behavior of compacted MX80 bentonite under constant water content conditions at elevated temperatures, simulating near-field conditions in nuclear waste repositories. Experiments were conducted using a high-pressure, high-temperature thermal triaxial cell capable of applying confining pressures up to 4 MPa and heating to 175 °C. The testing program consisted of staged heating–cooling cycles under 2 MPa and 4 MPa of isotropic confinement. Volumetric strain, pore air pressure, and temperature were continuously monitored. Raw displacement data were corrected for sensor thermal expansion and drift to isolate actual strains. Results indicate a clear transition from initial expansion to contraction at around 80 °C, followed by contractile creep at high temperature and negligible recovery upon cooling. Degree of saturation inferred from thermal strain evolution together with temperature effects on suction were used to infer effective stress changes. The experimental data were compared against the thermomechanical model proposed by Tang and Cui (2009), which accounts for temperature-dependent yield surfaces and suction effects within a double-structure elasto-plastic framework. Volumetric strains were correlated with net and effective stresses to identify yielding transitions. The model successfully captured key features of the thermal response, though minor discrepancies suggest the need for refinement under higher confinement. This work supports the validation and extension of constitutive models for compacted expansive clays under high temperatures that may be encountered in repositories with closely-spaced waste canisters.

1 INTRODUCTION

Compacted bentonite is widely used as a buffer material in deep geological repositories for high-level radioactive waste because of its low permeability, swelling capacity, and function as a barrier to radionuclide migration (Chijimatsu et al. 2000; Yang et al. 2021). In repository environments, heat emitted by waste canisters may raise bentonite temperatures well above 100 °C, inducing complex coupled thermo-hydro-mechanical (THM) processes. These include thermal expansion and contraction of the clay skeleton, vapor migration and desaturation, and stress redistribution within the pore structure (Cleall et al. 2013; Lu and McCartney 2022). Prediction of barrier performance requires an understanding of bentonite's volumetric response under elevated temperature and high stress confinement.

Laboratory studies have shown that thermal volumetric behavior under constant water content is nonlinear, with initial heating often producing slight expansion or limited contraction up to a threshold temperature (typically around 80 °C), followed by contraction at higher temperatures (Ye et al. 2012; Lu and McCartney 2023). However, most existing thermal volume change tests have been limited to temperatures below this threshold and under low confining pressures, leaving the high-temperature and moderate-stress response insufficiently characterized. In addition, interpretations often rely on total or net stress frameworks, which do not explicitly incorporate the evolving pore air pressure and suction that govern the effective stress on the soil structure (Alonso et al. 1990; Liu et al. 2021).

An effective stress-based interpretation, which combines pore air pressure and suction through a saturation-weighted formulation, provides a more comprehensive framework for describing thermal volume change. Tang and Cui (2009) proposed a constitutive model with independent stress state variables that incorporates temperature-dependent yield surfaces and suction effects within a double-structure elasto-plastic framework; however, its validation remains limited to low-temperature conditions. Extending this model to high-temperature applications requires experimental verification under relevant thermal and stress states.

In this study, thermal volumetric strains of compacted MX80 bentonite subjected to staged heating–cooling cycles under isotropic confining pressures of 2 MPa and 4 MPa, with peak temperatures up to 175°C. Volumetric strain, pore air pressure, and temperature were monitored continuously, and raw measurements were corrected to isolate actual deformations. Degree of saturation was inferred from the thermal strain response, which was used to estimate the suction using the soil-water retention curve (SWRC) and then interpret the effective stress framework. Finally, experimental results were compared with the model of Tang and Cui (2009) to evaluate its validity and identify areas for refinement under elevated thermal and mechanical loading conditions.

2 BACKGROUND

MX80 Bentonite from Wyoming is one of the most popular types of bentonites used internationally in bentonite buffer systems. The MX80 bentonite used in this work is supplied by American Colloid Company in granular form with an initial gravimetric water content of approximately 9%. The as-received granular form of bentonite when under low gravimetric water contents makes it have the appearance of sandy soil, but after hydration with water it will swell and develop the characteristic cohesion and appearance of a clay.

Understanding the thermo-hydro-mechanical (THM) behavior of compacted bentonite is essential for the long-term performance assessment of buffer barriers in deep geological repositories for high-level radioactive waste. In such environments, bentonite is subjected to complex coupled processes, including thermal loading due to radioactive decay, suction changes during hydration, and "mechanical

confinement from the surrounding host rock. These processes interact nonlinearly, especially under elevated temperatures and varying saturation degrees, challenging the applicability of conventional constitutive models. To model these coupled processes, it is necessary to develop constitutive frameworks capable of capturing the evolving volumetric behavior of soils under high-temperature and high-pressure conditions (Alonso et al. 1990; Liu et al. 2021).

Tang and Cui (2009) developed a thermo-mechanical constitutive model specifically aimed for compacted expansive clays under thermal loading. The model extends elasto-plastic formulations into a thermal domain by introducing temperature-dependent yield surfaces. It adopts a double structure concept, originally inspired by the Barcelona Basic Model (BBM) proposed by Alonso et al. (1990), in which the soil fabric is divided into macrostructural and microstructural components. The total void ratio e is expressed as:

$$e = e_m + e_M \quad (1)$$

where e_m is the microstructural void ratio and e_M is the macrostructural void ratio. The microstructure is assumed to remain saturated and resilient to temperature changes, while irreversible deformation and thermal contraction are governed by macrostructural behavior.

The microstructural elastic volumetric strain is given by:

$$d\varepsilon_v m^e = de_m/(1+e_m) = d(p+s)/K_m + \alpha_m^T dT \quad (2)$$

where p is the net mean stress, s is matric suction, K_m is the microstructural bulk modulus, and α_m^T is the microstructural coefficient of thermal expansion. The macrostructural elastic volumetric strain is:

$$d\varepsilon_v M^e = de_M/(1+e_M) = \kappa/(1+e_M)(dp/p) + \kappa_s/(1+e_M)\big(ds/(s+p_{atm})\big)\alpha_m^T dT \quad (3)$$

where κ and κ_s are elastic compressibility parameters for changes in p and s, p_{atm} is atmospheric pressure, and α_m^T is the macrostructural coefficient of thermal expansion.

The microstructural response is treated as elastic, whereas irreversible deformation and thermal contraction are governed by macrostructural behavior. This separation enables the model to distinguish between reversible swelling from water redistribution and permanent deformation induced by stress or temperature beyond yield thresholds.

The model proposed by Tang and Cui (2009) incorporates two coupled yield surfaces: one in the suction–stress space and another in the temperature–stress space. The suction–stress yield surface controls mechanical plasticity, while the temperature–stress yield surface governs the start of thermal plastic strain. Plastic macrostructural strain under mechanical loading is given by:

$$d\varepsilon_v ML^p = [\lambda(s) - \kappa]/(1+e_M) * (dp_0/p_0) \quad (4)$$

where $\lambda(s)$is the virgin compression index at suction s, and p_0 is the net mean yield stress. Micro–macrostructural interaction under suction increase (SI) or decrease (SD) produces:

$$d\varepsilon_v MSI^p = f_I d\varepsilon_v m^e \quad (5)$$

$$d\varepsilon_v MSD^p = f_D d\varepsilon_v m^e \quad (6)$$

where $f_I$and f_D are interaction functions for SI and SD.

Thermal expansion is considered elastic until the temperature reaches a threshold—referred to as the thermal yield temperature—beyond which plastic contraction begins. Plastic macrostructural strain due to thermal yielding is:

$$d\varepsilon_v MT^p = -\alpha_M^T/(1-a)(exp\big[-\alpha_M^T/(1-a)\big(T - T_{CT}{}^0\big)\big] - a)T \quad (7)$$

where a is a shape parameter and $T_{CT}{}^0$ is the initial thermal yield temperature. The total macrostructural plastic volumetric strain is:

$$d\varepsilon_v M^p = d\varepsilon_v MT^p + d\varepsilon_v ML^p + d\varepsilon_v MSI^p + d\varepsilon_v MSD^p \quad (8)$$

This mechanism enables the model to simulate both the initial expansion and subsequent contraction observed in experiments during heating under constant water content (Tang and Cui 2009; Ye et al. 2012). Importantly, the thermal yield boundary evolves with suction and net mean stress, reflecting the progressive thermal softening of the material.

One of the model's key innovations is the inclusion of a temperature-dependent reduction in the net mean yielding stress. As the temperature increases, the yield surface in the mechanical domain shrinks, representing the experimentally observed decrease in strength and stiffness with thermal exposure (Tang and Cui 2009). This feature has been shown to reproduce laboratory observations of thermal contraction, where high-temperature loading leads to volumetric contraction even in unsaturated specimens held under constant suction (Ye et al. 2012; Lu and McCartney 2023).

Despite its robust formulation, the original model was primarily validated using laboratory heating tests on MX80 bentonite at temperatures up to 80 °C under low confining stresses (typically <0.5 MPa). These conditions do not fully reflect the stress and temperature levels expected in deep geological repositories, where bentonite barriers may be subjected to isotropic stress conditions on the order of 2 to 5 MPa and thermal loads exceeding 150 °C. Several studies have highlighted the need to extend validation efforts to higher thermal and mechanical regimes (Chijimatsu et al. 2000; Liu et al. 2021; Yang et al. 2021). Under high temperature and moderate-to-high stress levels, the role of suction becomes more complex, and the assumption of constant water content may no longer hold due to thermally induced vapor migration and pore pressure redistribution (Cleall et al. 2013; Lu and McCartney 2022).

Another limitation of the existing model application lies in the difficulty of interpreting measured thermal strain using total stress or net stress frameworks. These stress measures neglect the evolving suction and partial saturation, which strongly influence the mechanical response of unsaturated bentonite. A more comprehensive interpretation requires adopting an effective stress framework that accounts for the contributions of both pore air pressure and suction. This approach has been advocated in numerous recent studies on unsaturated soil mechanics (Alonso et al. 1990; Liu et al. 2021), particularly under variable saturation and temperature conditions. By incorporating effective stress into the analysis, it becomes possible to better quantify the role of suction softening, identify the yield point, and assess the applicability of constitutive models like those of Tang and Cui (2009) under field-relevant conditions.

Lu and McCartney (2022, 2023) demonstrated that thermal gradients can induce water redistribution between macro- and micro-pores, influencing both suction and degree of saturation. These mechanisms are not fully captured in traditional constitutive models and may contribute to discrepancies between predicted and observed volumetric behavior at high temperatures. Similarly, experimental work by Ye et al. (2024) emphasized the temperature dependence of thermal conductivity and its influence on transient heat transfer, which may indirectly affect strain measurements and thermal equilibrium times.

The present study aims to fill this gap by experimentally investigating the thermal volumetric response of compacted MX80 bentonite under isotropic confining pressures of 2 MPa and 4 MPa, with heating up to 175 °C. The data are analyzed using an effective stress framework to evaluate the temperature-dependent yield behavior and to assess the applicability of Tang

and Cui's model under elevated THM conditions. In addition to characterizing thermal volumetric strain, the study focuses on the evolution of effective stress, porosity, and degree of saturation during heating and cooling cycles. Thermal yield points are identified and compared with model predictions to evaluate the validity and limitations of the original formulation under high-temperature regimes. By extending model validation beyond 80 °C and moderate stress levels, this work provides new experimental evidence to support the applicability of the effective stress concept in predicting thermal contraction behavior in bentonite buffers.

3 EXPERIMENTAL PROGRAM

The granular MX80 bentonite (initial water content ≈ 9%) was sieved (< 0.5 mm), humidified to 13%, and statically compacted into cylinders (71.32 mm × 70.35 mm). Tests were conducted in a custom thermal isotropic cell (max. 20 MPa, 200 °C) with silicone-oil confinement, a heating jacket, embedded thermocouples, and high-temperature LVDTs for axial/radial strain measurement. The specimen was isotropically loaded to 2 MPa at room temperature, heated stepwise to 175 °C, then cooled; a second cycle was performed at 4 MPa using the same heating–cooling protocol. Details on the experimental setup can be found in Liu et al. (2026).

4 RESULTS

The full-time histories of the test are compiled in Figure 1, which displays (a) cell pressure, (b) pore air pressure, (c) specimen temperature, and (d) cumulative volumetric strain. First, the specimen was isotropically loaded to 2 MPa at room temperature and held at that stress for the first thermal cycle. Axial (ε_a) and radial (ε_r) LVDT readings were combined to obtain volumetric strain as follows:

$$\varepsilon_v = \varepsilon_a + 2\varepsilon_r \quad (9)$$

Figure 1(a) shows the two discrete loading steps: an initial rise to 2 MPa and, after cooldown, a second step to 4 MPa. The specimen-internal temperature plotted in Figure 1(c), the data was recorded by the embedded thermocouples, it raised from ~25 °C in 25 °C increments to a peak of around 150 °C held long enough for thermal equilibrium within the sample, and then gradually reduced to room temperature. A second heating–cooling cycle under 4 MPa confinement followed, with the specimen temperature heated up to 140 °C, then entered the cooling stage, and data were collected down to about 75 °C, where the record for this cycle ends.

The pore air pressure response in Figure 1(b) mirrored the temperature program, climbing to 0.33 MPa during the first heating phase, reduced slightly during the high-temperature hold, and returned to near-atmospheric values on cooldown. A similar peak of 0.29 MPa occurred in the second cycle.

Volumetric-strain evolution shows in Figure 1(d) reveals the coupled thermo-mechanical behavior. Loading to 2 MPa produced an instantaneous compression of –0.8 %. Subsequent heating generated a modest reversible expansion up to 80 °C, followed by progressive contraction that reached ≈–5.0% at the equilibrium status of 150 °C. Cooling induced negligible elastic rebound, leaving a residual strain of –5.2 %. Increasing the confining pressure to 4 MPa caused an additional mechanical compression of –2.3 %; the second thermal cycle then produced only ≈–1.1 % further contraction, with a final residual strain of –1.3 %. These trends confirm that higher isotropic stress markedly suppresses thermally induced contraction.

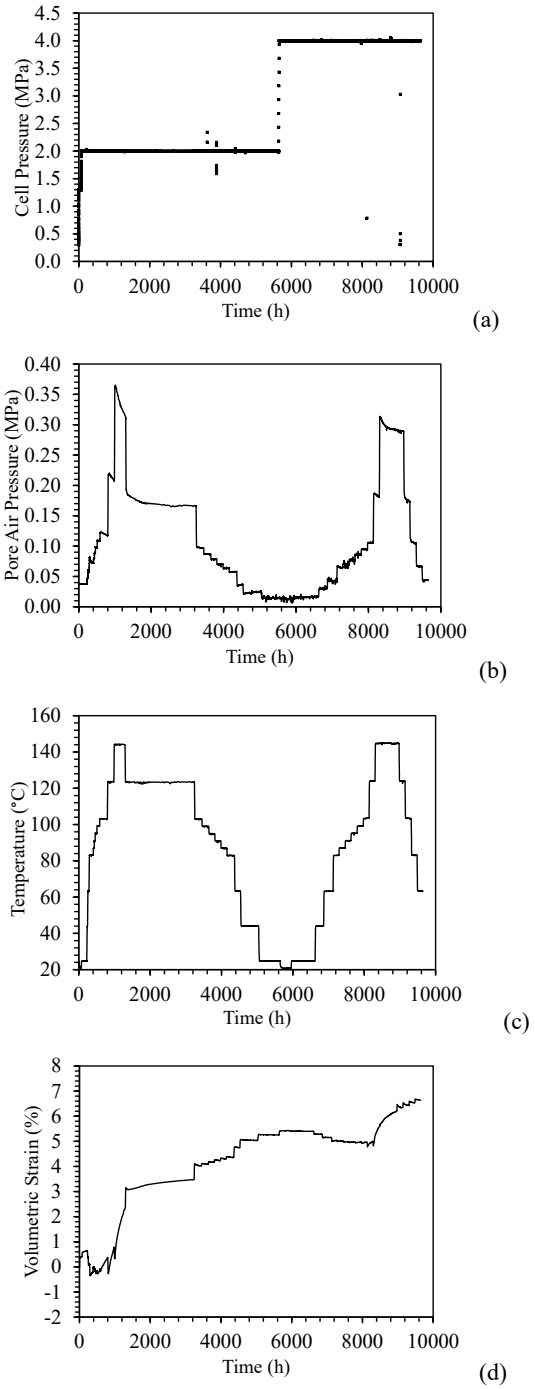

Figure 1. Time series of measured variables: (a) Cell pressure; (b) Pore air pressure; (c) Temperature; (d) Volumetric strain

Figure 2 presents the time evolution of the variables inferred from the raw measurements: (a) matric suction and (b) degree of saturation, both derived from the pore air pressure and volumetric-strain histories shown in Figure 2. Suction rises sharply during the first heating cycle, climbing from an initial value of 38 MPa to a peak of 46 MPa as temperature approaches 150 °C. The increase reflects the combined effects of pore-fluid thermal expansion and progressive contraction of the clay skeleton under constant water content. Once the temperature equilibrium status is reached, suction remains nearly constant for several hundred hours, then drops steadily during cooldown, stabilizing at 39 MPa.

When the confining pressure is raised to 4 MPa the suction curve again mirrors the temperature program, increasing to 47 MPa at the 140 °C peak and falling as the specimen cools down. The final recorded value of suction at 75 °C is 41 MPa. The slightly higher peak suction under 4 MPa confinement confirms that denser microstructure and smaller void ratio produce a larger thermal pressure build-up.

The corresponding degree of saturation trajectory in Figure 2(b) shows a gradual decline from an initial 0.496 to 0.445 over the first thermal cycle, owing to the volumetric expansion of the pore space at constant water mass. Minor step-like drops coincide with each temperature increment, while the long isothermal hold produces only limited additional change. During the second cycle, saturation remains nearly constant as the specimen is heated to 140 °C, then slightly decreased to 0.429 during the cooling stage to 75 °C. These trends demonstrate that thermal contraction of the void structure, combined with irreversible contraction, systematically reduces saturation even though no external fluid exchange is permitted.

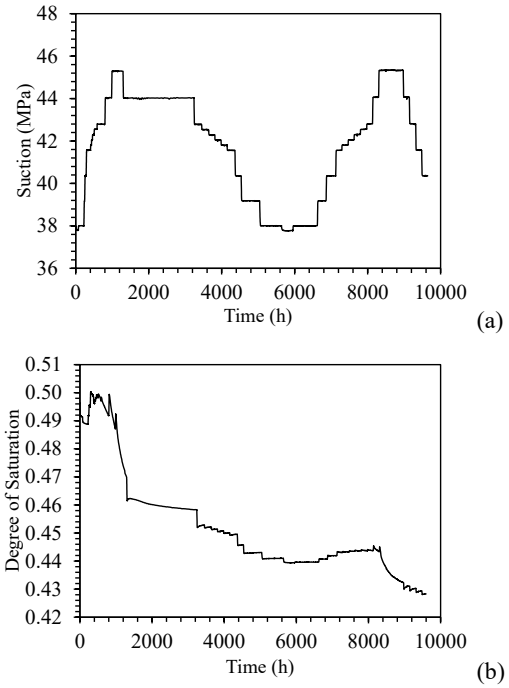

Figure 2. Time series of inferred variables: (a) Suction; (b) Degree of saturation

The triaxial THM cell provides two independent stress readings of total stress (σ_{cell}), which is the confining (cell) pressure recorded by the oil-line pressure transducer. Pore air pressure (u_a) is the internal air pressure measured by the miniature high-temperature pressure sensor installed in the specimen. For the constant-water-content tests performed here, effective stress was assessed in two convenient forms: Total stress acts on the specimen boundary and is defined as as follows for a test in an isotropic cell:

$$\sigma_{total} = \sigma_{cell} \quad (10)$$

The net mean stress is transmitted through the soil skeleton after subtraction of the measured air pressure, as follows:

$$\sigma_{net} = \sigma_{cell} - u_a \quad (11)$$

The effective stress can then be defined as follows:

$$\sigma' = (\sigma_{cell} - u_a) + \chi\psi \quad (12)$$

where χ is assumed to equal the degree of saturation S, and ψ is the matric suction.

Figure 3 documents the void-ratio response during the 2 MPa cycle. Figure 3(a) plots void ratio e against mean net stress σ_{net}, Figure 3(b) plots the same data versus mean effective stress σ'. The specimen starts at an initial void ratio $e_0 = 0.719$. Isotropic loading to 2 MPa produces mechanical compression. As temperature rises, the curve first moves slightly upward because of thermal expansion until the specimen temperature reaches roughly 80 °C; beyond this point the curve drops steeply, indicating thermal contraction. Cooling drives the state leftwards in stress space but produces almost no upward rebound, so the test terminates at a final void ratio $e_f = 0.635$. Figure 3(b) presents the same void ratio data against effective stress. Relative to Figure 3(a), the curve is noticeably steeper and more confined laterally: the initial loading step appears as a short vertical drop, the heating path descends with only a modest right-hand drift, and the cooling leg rises nearly along the same line. Overall, the e–σ′ curve forms a narrow, column-like band, illustrating that the horizontal spread visible in the net-stress plot is greatly reduced for the effective stress.

Figure 4 depicts the void-ratio response during the 4 MPa cycles. The stage begins at an initial void ratio $e_0 = 0.635$. Increasing the cell pressure from 2 MPa to 4 MPa produces a slight vertical drop to $e = 0.629$. Subsequent heating to roughly 140 °C first introduces an expansion leading to an increase of void ratio to $e = 0.645$, then decreases to $e = 0.616$. In the net-stress plot this appears as a slight rightward-and-downward drift, whereas in the effective-stress plot the same points trace an almost vertical line on the log-linear plot, spanning a narrow effective stress interval. Cooling retraces that steep path with virtually no rebound, and the cycle terminates at $e_f = 0.605$. Compared with the 2 MPa results, the 4 MPa curves are noticeably steeper and laterally compressed, underscoring that higher isotropic stress greatly restricts additional thermally induced contraction. Continuous yielding is observed after reaching a void ratio of 0.645 leading to contraction during heating to elevated temperature, followed, by elastic contraction during cooling. Overall, the interpretation of the volume change results indicates that an elasto-plastic framework is required to interpret the thermally-induced volume change.

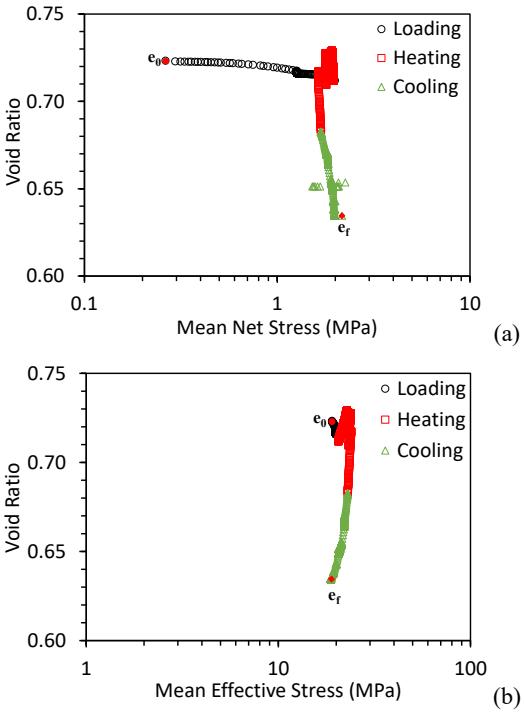

Figure 3. Void ratio versus stress under 2 MPa: (a) Net stress (b) Effective Stress

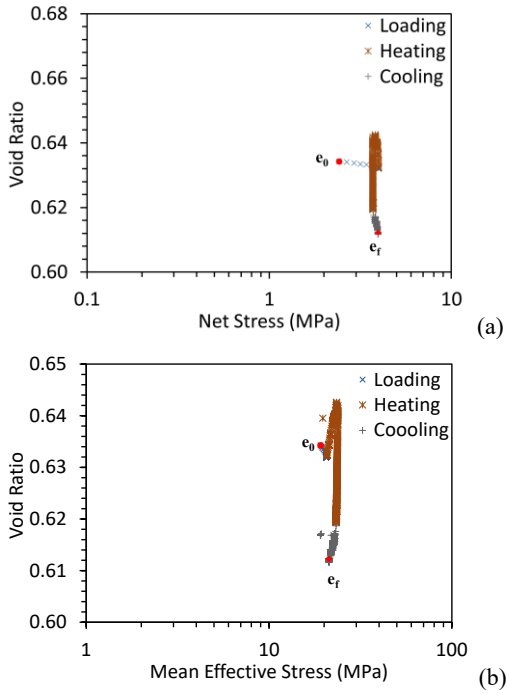

Figure 4. Void ratio versus stress under 4 MPa: (a) Net stress (b) Effective stress

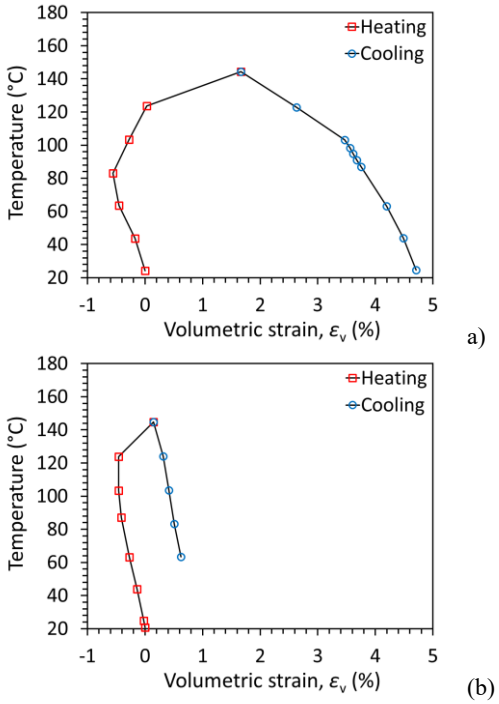

Figure 5. Equilibrium thermal volume change of compacted bentonite versus temperature: (a) 2 MPa isotropic loading; (b) 4 MPa isotropic loading

Figure 5 shows the equilibrium points on the ε_v–T paths for the two confining stresses and shows how both the sign and magnitude of thermal volumetric strain depend on isotropic pressure. For 2 MPa, the specimen is referenced to zero strain at 24 °C. Heating first drives a progressive contraction: ε_v falls to –0.17 % at 44 °C, –0.45 % at 64 °C and reaches its minimum of –0.56 % at 83 °C, which is the temperature of the contraction–swell inversion point. Beyond 83 °C the trend reverses, the soil begins to expand, recovering to –0.08 % at 103 °C, crossing into positive strain at 124 °C, and peaking at +1.66 % at 144 °C.

During cooling the expansion continues: ε_v climbs to 2.63 % at 123 °C, then rises step-wise to 3.75 % at 87 °C and culminates at 4.71 % upon returning to 25 °C. The 2 MPa cycle therefore records an initial contraction of 0.56 % followed by a net swell of roughly 5.3 %. Under 4 MPa confinement (Figure 5b) the behaviour is subdued. Contraction persists up to about 124 °C, where the minimum strain of –0.46 % is observed. Only at the maximum temperature of 145 °C does expansion set in, reaching 0.15 %. Cooling produces a modest recovery, and ε_v stabilises at 0.62 % by 63 °C. Compared with the low-pressure cycle, both the contraction magnitude and the overall swell are dramatically reduced.

5 ANALYSIS

The relationship between volumetric strain and temperature for the specimen tested under a net mean stress of 2 MPa is shown in Figure 6, together with the simulation results obtained from the model of Tang and Cui (2009). The fitted curve closely reproduces the initial expansion and contraction, successfully predicting the temperature range for the transition from expansion to contraction, and accurately following the contraction trend up to the maximum temperature. The calibrated parameters used in the simulation are summarized in Tables 1 and 2, which present the initial state variables, hydromechanical properties, and thermal properties adopted in the model.

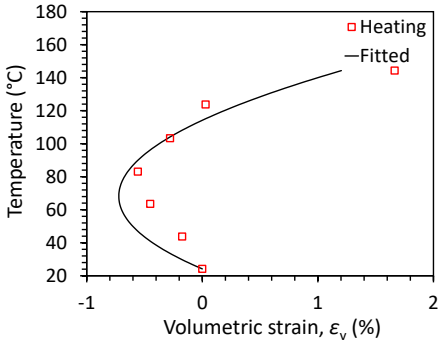

Figure 6. Model fitting of volumetric strain versus temperature under 2 MPa during heating

Figure 7 compares the experimental volumetric strain–temperature response at 4 MPa with the model prediction obtained without additional calibration. The simulation uses the same parameter set established for the 2 MPa fit. The data exhibit contraction from the beginning of heating, whereas the prediction overpredicts the thermal expansion in the low-temperature range. The transition from expansion to contraction occurs earlier in the experiment than in the model prediction, indicating that the model places the thermal yield onset at a temperature that is too high for this stress state, although drainage was not allowed in the test during application of the greater cell pressure (the mechanical compression response was not drained). At higher temperatures the predicted curve becomes overly expansive relative to the data, leading to a positive bias in the high temperature range. Together, these features suggest that the transferred parameter set does not fully capture the stronger pressure dependence of thermal yielding and the thermal volume change at 4 MPa. An earlier thermal yield at higher mean net stress and a smaller contraction at elevated temperature would be consistent with the measurements. Within the present framework this would correspond to a modest increase in the parameters governing the thermal yield and a slight reduction in the macrostructural thermal expansion coefficient α_m^T to limit the high-temperature

contraction, with only minor adjustments to the elastic compressibility values of κ and $\lambda(0)$ if additional stiffening is required.

Table 1. Initial state parameters

Parameter	Symbol	Value	Unit
Initial total void ratio	e	0.723	–
Initial macrostructural void ratio	e_M	0.323	–
Initial microstructural void ratio	e_m	0.400	–
Reference temperature	T_0	25.00	°C
Initial suction	s_0	39	MPa
Net mean yield stress at reference temperature	p_0*	0.5	MPa
Initial applied net mean stress	p_{ini}	0.1	MPa

Table 2. Thermo-hydro-mechanical parameters

Parameter	Symbol	Value	Unit
Elastic compressibility index for net mean stress	κ	0.008	–
Elastic compressibility index for suction	κ_s	0.077	–
Virgin compression slope at zero suction	$\lambda(0)$	0.25	–
Suction effect control parameter	p_c	0.25	MPa
Shape parameter of suction–yield surface	r	0.18	–
Suction dependency parameter of $\lambda(s)$	β	0.14	–
Microstructural stiffness parameter	α_m	0.0617	MPa^{-1}
Suction effect on microstructure	β_m	−0.0167	MPa^{-1}
Atmospheric pressure	p_{atm}	0.1013	MPa
Thermal expansion coefficient for microstructure	α_m^T	−0.0001	$°C^{-1}$
Thermal expansion coefficient for macrostructure	α_M^T	−0.0001	$°C^{-1}$
Thermal yield temperature dependency parameter	α_0	0.01	$°C^{-1}$
Reference temperature for thermal yield	T_c	200	°C
Suction dependency of thermal yield	α_s	0.016	MPa^{-1}
Shape parameter of thermal yield curve	β_T	0.9	–
Post-yield thermal contraction rate parameter	α	1.037	–

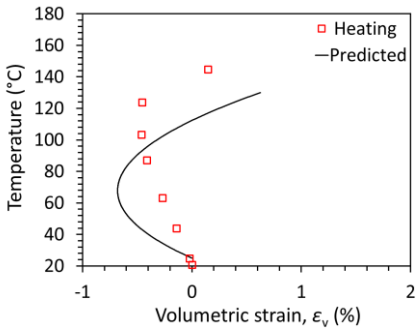

Figure 7. Model prediction of volumetric strain versus temperature under 4 MPa during heating

6 CONCLUSIONS

Higher confinement markedly suppressed thermal contraction, and the thermal response was interpreted within an effective stress framework using inferred suction and degree of saturation. This approach significantly reduced the apparent lateral spread of void-ratio–stress curves compared with net stress representation, highlighting its suitability for unsaturated bentonite under high-temperature loading. The observed thermal yield points, suction evolution, and residual strains provide valuable benchmarks for constitutive model calibration.

Comparison with the thermo-mechanical model of Tang and Cui (2009) indicate that the thermo-elasto-plastic approach can successfully reproduce the general trends of thermal expansion–contraction behavior, including the temperature-dependent yield surface shifts. However, discrepancies emerged under higher confinement, particularly in capturing the magnitude of thermal contraction and residual strains, suggesting the need for refinement to better account for pore structure effects and suction evolution at elevated temperatures.

Further research is needed into the role of effective stress and the changes in stress state induced by temperature. These findings provide experimental evidence that can improve predictive models of bentonite buffer performance, thereby supporting the reliable design of engineered barrier systems for high-level radioactive waste disposal.

7 ACKNOWLEDGEMENTS

The authors appreciate support from U.S. Dept. of Energy Nuclear Energy University Program award DE-NE0009460. The views in this paper are those of the authors alone.

8 REFERENCES

Alonso, E.E., Gens, A., and Josa, A. (1990). “A constitutive model for partially saturated soils,” Géotechnique, vol. 40, no. 3, pp. 405–430, doi: 10.1680/geot.1990.40.3.405.

Chijimatsu, M., Fujita, T., Kobayashi, A., and Nakano, M. (2000). “Experiment and validation of numerical simulation of coupled thermal, hydraulic and mechanical behaviour in the engineered buffer materials,” Int. J. Numer. Anal. Methods Geomech., vol. 24, no. 4, pp. 403–424.

Cleall, P.J., Singh, R.M., and Thomas, H.R. (2013). “Vapour transfer in unsaturated compacted bentonite,” Géotechnique, vol. 63, no. 11, pp. 957–964.

Liu, X., Behbehani, F., Lu, Y., and McCartney, J.S. (2026). “Effective stress evaluation of the thermal volume change of swelling soils”. GeoCongress 2026. Salt Lake City. ASCE, Reston, VA. 10 pg.

Liu, Y., Cai, G., Zhou, A., Han, B., Li, J., and Zhao, C. (2021). “A fully coupled constitutive model for thermo-hydro-mechanical behaviour of unsaturated soils,” Comput. Geotech., vol. 133, p. 104032.

Lu, Y. and McCartney, J.S. (2022). “Physical modeling of coupled thermo-hydraulic behavior of compacted MX80 bentonite during heating.” Geotechnical Testing Journal. 45(6), 20220054.

Lu, Y. and McCartney, J.S. (2023). “Insights into the thermo-hydraulic properties of compacted MX80 bentonite during hydration under elevated temperature.” Canadian Geotechnical Journal. 61(2), 344-360.

Lu, Y. and McCartney, J.S. (2024). “Transient temperature and water distributions in unconstrained compacted granular bentonite under elevated temperatures.” Geomechanics for Energy and the Environment. 41, 100626.

Tang, A.-M. and Cui, Y.-J. (2009). “Modelling the thermomechanical volume change behaviour of compacted expansive clays,” Géotechnique, vol. 59, no. 3, pp. 185–195.

Yang, G., Liu,, Y., Gao, Y., Li, J., and Cai, G. (2021). “Coupled thermo-hydro-mechanical process in buffer material and self-healing effects with joints.” J. Cent. S. Uni., vol. 28, no. 9, pp. 2905–2918.